High Temporal Resolution Polarimetric Radar Observations of the 20 May 2013 Newcastle-Moore, Oklahoma EF-5 Tornado using the PX-1000

James M. Kurdzo[1,2], David J. Bodine[3], Boon Leng Cheong[2], and Robert D. Palmer[1,2]

[1]*Advanced Radar Research Center, University of Oklahoma, Norman, Oklahoma*
[2]*School of Meteorology, University of Oklahoma, Norman, Oklahoma*
[3]*Advanced Studies Program, National Center for Atmospheric Research, Boulder, Colorado*

ABSTRACT

On 20 May 2013, the cities of Newcastle and Moore, Oklahoma were impacted by a long-track violent tornado that was rated as an EF-5 on the enhanced Fujita scale by the National Weather Service. A plethora of radar systems in and around the Norman/Oklahoma city area observed this tornado and its parent supercell at varying distances and with varying scanning strategies and capabilities. Despite a relatively sustained long track, damage surveys revealed a number of small-scale debris features that hint at storm-scale processes that occurred over very short time periods. The University of Oklahoma Advanced Radar Research Center's PX-1000 transportable, polarimetric, X-band weather radar was operating in a single-elevation PPI scanning strategy at the OU Westheimer airport throughout the duration of the tornado, collecting high spatial and temporal resolution polarimetric data every 20 s at ranges as close as 10 km and heights below 500 m AGL. This unique dataset contains the only known polarimetric radar observations of the Newcastle-Moore tornado at such high temporal resolution, providing the opportunity to analyze and study fine-scale phenomena occurring on very rapid time scales. This paper specifically analyzes a series of debris ejections and rear flank downdraft surges that both preceded and followed a distinctive loop of the core tornadic vortex as it weakened over the Moore Medical Center before rapidly accelerating and re-strengthening to the east. The gust front structure, debris/hydrometeor microphysics, and Z_{DR} arc breakdown are explored as strong evidence for a "failed occlusion." A conceptual description and illustration of the failed occlusion hypothesis is provided, and its implications are discussed.

1. Introduction

The 20 May 2013 EF5 tornado that affected Moore, Oklahoma was observed by numerous radar systems in and around the Oklahoma City area with varying spatial/temporal resolutions, distances/angles to the storm, and capabilities. The University of Oklahoma Advanced Radar Research Center's PX-1000 transportable, polarimetric, X-band radar combined temporal resolution of 20 s and oversampled spatial resolution of 30 m in range and 1° in azimuth with high-quality polarimetric estimates and relatively close range to form a distinct perspective regarding fine-scale phenomena in the storm.

The Moore storm was the subject of the most detailed storm survey in National Weather Service (NWS) history, consisting of more than 4,200 damage indicators (Atkins et al. 2014; Burgess et al. 2014). Of particular interest in the damage survey results was the path of the tornado in the vicinity of the Moore Medical Center (MMC), where a distinct loop was observed. During analysis of PX-1000 data, a number of fine-scale shifts in the track of the tornado were discovered that were not readily apparent in the damage survey. This study analyzes these track shifts, forward speed changes, debris ejections (and their relation to rear-flank gust front surges or RFGFSs), and polarimetric tornadic debris signatures (TDSs; Ryzhkov et al. (2002, 2005)) in order to differentiate/compare each of the observed shift instances with the observed loop at the MMC.

Comparisons between RFGFSs and mesocyclone structure have been a common research theme in recent years (Adlerman et al. 1999; Finley and Lee 2004; Adlerman and Droegemeier 2005; Skinner et al. 2014), as has the comparison between RFGFSs and ongoing tornadic debris (Houser 2013; Houser et al. 2014). The Moore storm displayed numerous instances of RFGFSs and subsequent debris ejections, however these surges occurred on extremely rapid time scales and did not result in tornadogenesis or tornadic dissipation. The single instance of near-occlusion is of particular interest among the RFGFSs. Section 2 of this paper presents

Corresponding author address: James M. Kurdzo, Advanced Radar Research Center, University of Oklahoma, 3190 Monitor Avenue, Norman, OK 73019.
E-mail: kurdzo@ou.edu

the PX-1000 system, and Section 3 discusses the event overview. Sections 4 and 5 present a detailed overview of the PX-1000 dataset and a discussion of its implications, respectively, while Section 6 offers a summary and some concluding remarks.

2. PX-1000 System Description

The PX-1000 radar is a transportable, polarimetric, X-band, dish-based platform mounted on a trailer (Cheong et al. (2013)). PX-1000 operates at 100-W peak power, and the pulse compression scheme described in Kurdzo et al. (2014) is used in order to achieve the necessary sensitivity for meteorological data collection. The resulting sensitivity is approximately 14 dBZ at 50 km range, and the native range resolution is 112 m. The 1.8-m diameter parabolic dish results in a 1.8° azimuthal resolution at 9.55 GHz. The range gates and azimuths are oversampled to 30 m and 1.0°, respectively.

Before the onset of severe weather on 20 May, PX-1000 was set to run at a constant 2.6° elevation (PPI) scan at a rotation rate of 18° s^{-1}, resulting in an update rate of 20 s. Although other scanning strategies would have been useful for various types of analysis (e.g., volumetric analysis), the 20-s update rate, even at a single elevation, resulted in a polarimetric dataset capable of detecting rapidly evolving areas of the storm that a volumetric scanning strategy would have missed.

PX-1000 I/Q data were processed with a time-frequency multiplexed matched filter to generate moment data. Velocity dealiasing was completed manually using standard unfolding techniques. Attenuation correction was applied to the data using differential attenuation parameterizations (Bringi et al. 1990; Jameson 1992; Park et al. 2005). The values suggested by Snyder et al. (2010) at X-band were used for correction of Z_{HH} and Z_{DR}. The convergence (δ) calculations were formulated using the single-Doppler v_r field from PX-1000.

3. Event Overview and Tornado Track

The first radar returns of the Moore storm appeared at approximately 1900 UTC, west of Bridge Creek. By 1934 UTC, three distinct cells and associated mesocyclones were evident, with one near Mustang, a second east of Tuttle, and a third just north of Bridge Creek. By 1946 UTC, the northern cells had dissipated, and the southern cell had strengthened, with a hook structure in horizontal reflectivity factor (Z_{HH}) and a ~60 m s^{-1} inbound/outbound radial velocity differential (Δv_r) across the mesocyclone (spanning ~2 km). Between 1946–1956 UTC, a surge of precipitation occurred around the base of the hook, with tornadogenesis estimated at 1956 UTC according to the NWS damage survey (Burgess et al. 2014). Gate-to-gate PX-1000 Δv_r at tornadogenesis was ~35 m s^{-1}. A low-Z_{HH} region and a polarimetric debris signature quickly became evident in low-level scans.

The tornado rapidly strengthened, producing EF3-EF4 damage within four minutes of tornadogenesis. A series of Z_{HH} and v_r examples from key times during the tornado are shown in Fig. 1, as well as the PX-1000-indicated tornado track and the contoured maximum EF-scale damage ratings from Burgess et al. (2014). From 2014–2023 UTC, a constant swath of EF4 damage, with occasional EF5 damage, was evident in the damage survey. As seen in the PX-1000 data, the tornado shifted east and north multiple times before turning sharply to the north and looping just west of the MMC at I-35 between 2023–2024 UTC. After this loop, Δv_r decreased and forward ground speed increased, but consistent EF3 (and common EF4) damage continued through approximately 2030 UTC, with dissipation occurring around 2035 UTC. The NWS survey indicated that the tornado lasted 39 minutes and had a path length of 23 km and a maximum damage width of 1.7 km. Of the 4,531 damaged structures, over 3,500 were residential buildings (Atkins et al. 2014), and more than 300 structures experienced EF4/EF5 damage (Burgess et al. 2014).

4. PX-1000 Radar Observations

a. RFGF Surges and Debris Ejections

Throughout the lifetime of the Moore tornado, a series of track shifts and debris ejections were observed in the PX-1000 data. Debris ejections in this context are defined as an area of debris ejected from the core tornado vortex along a line typically to the south of the tornado and have been referred to as debris "tails" or debris deformation events in previous studies (Houser 2013; Houser et al. 2014). Debris ejections are differentiated from the TDS by an asymmetry in the TDS with a non-debris separation between the TDS and the tail necessary for identification. A conceptual diagram of debris ejections/tails is provided in Fig. 2.

As with debris in a TDS, polarimetric radar can be used to mark debris in an ejection by identify-

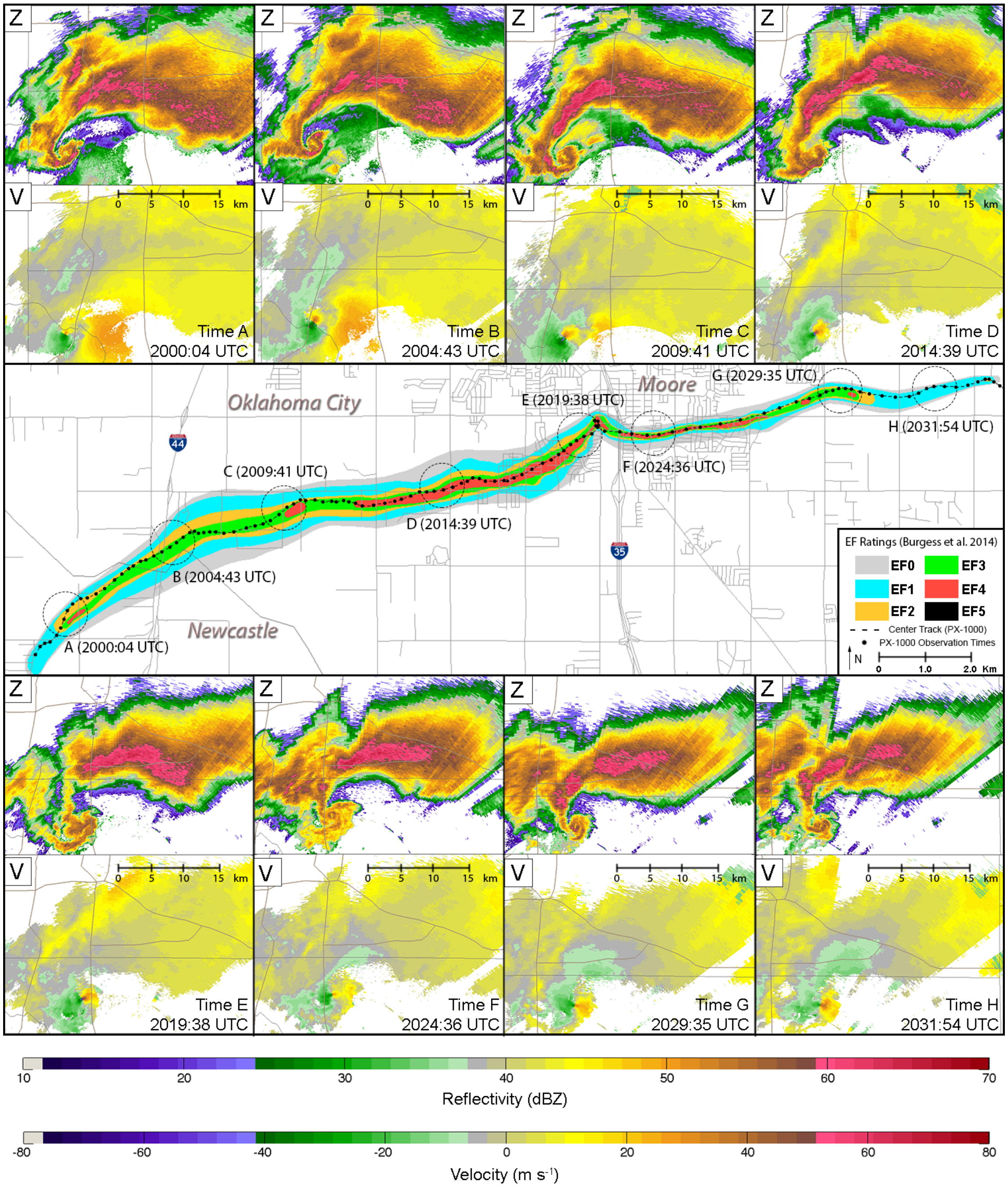

FIG. 1. EF-scale damage ratings (colored shading, from Burgess et al. (2014)), vortex center track from PX-1000 Δv_r data (dotted black line), PX-1000 observation times (black dots), and sample Z_{HH} and v_r data from different times/locations along the tornado track shown in top/bottom frames (denoted by circles and times A-H).

ing relatively low values in $\rho_{\rm HV}$ and $Z_{\rm DR}$, and relatively high values in $Z_{\rm HH}$. Bodine et al. (2013) suggest that debris at S-band can be differentiated using $Z_{\rm HH}$ values greater than 42.5 dBZ co-located with $\rho_{\rm HV}$ values below 0.825. These thresholds have been applied to the PX-1000 data at X band in order to locate debris inside and outside the tornadic circulation with the expectation that the values will yield viable results at X-band. Furthermore, it is contended that debris tails have a direct association with RFGFSs, since a surge of high winds would be likely to carry debris from the tornadic circulation, especially in strong tornadoes in populated areas that contain a significant amount of debris (Fig. 2). Additionally, a RFGFS implies an intensification of the downdraft, which would likely enhance debris fallout into the RFD. While the analysis of RFGFSs with high-temporal and high-spatial resolution dual-Doppler observations would be ideal, the lack of radar datasets in the Oklahoma City metropolitan area on 20 May with the temporal resolution of PX-1000 makes this type of analysis in the Moore tornado impossible, especially due to the fact that many of the debris ejections observed existed on time scales less than 1–2 min. Therefore, for the Moore case, it is argued that the PX-1000 observations of debris ejections can be used as a proxy to analyze RFGFSs at high temporal resolution. It can be argued that each of the debris ejections was associated with a δ maxima, suggesting that near-surface convergent flow along RFGFSs caused debris lofting and therefore, a manifestation of each RFGFS in the $\rho_{\rm HV}$ field.

Assuming this is true for all observed debris ejections throughout the lifetime of the Moore tornado, a series of RFGFSs can be analyzed using the high resolution PX-1000 polarimetric data. The debris ejections (or RFGFSs) occurred regularly along the track of the tornado and often preceded track shifts; they are referred to as R1-R8 in the following sections. With the lack of high-temporal resolution dual-Doppler observations, the existence of debris in "tail" shapes can be used to analyze characteristics of the RFGFSs. By manually tracing the RFGFS signatures and thresholding for $Z_{\rm HH}$ and $\rho_{\rm HV}$ values consistent with debris, radar gates associated with RFGFS debris can be compared in direction to the tornado location in a moving reference frame. These

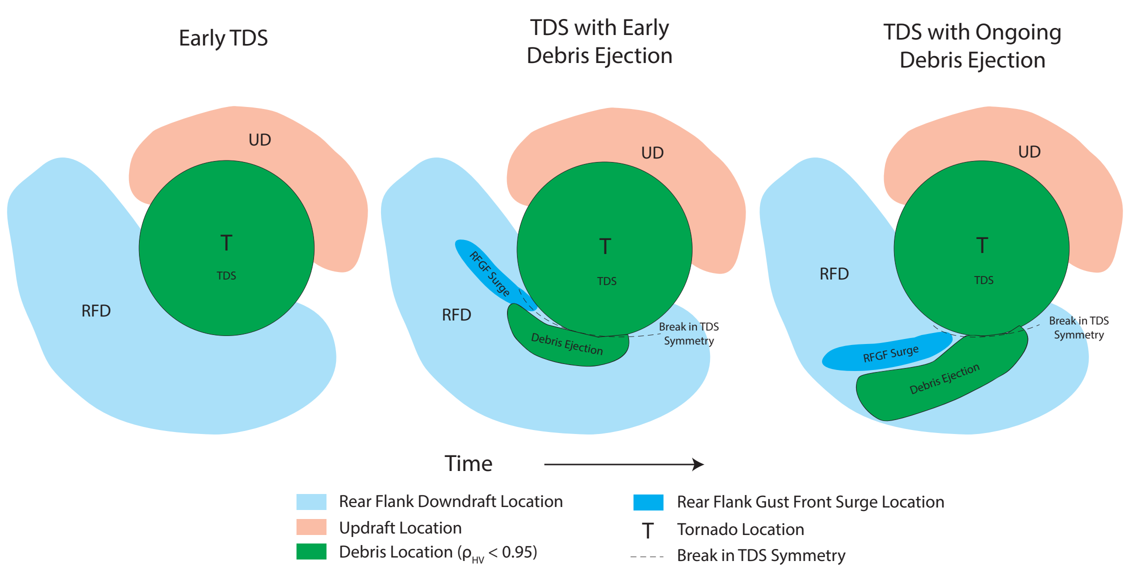

Fig. 2. Conceptual diagram of the debris ejection process. The early stages of the tornado (left) display a typical $\rho_{\rm HV}$ minimum within the TDS. As the tornado matures (center), the RFD develops a concentrated area of high low-level winds marking a RFGFS and a debris ejection. The debris ejection/RFGFS is qualitatively defined as a debris "tail" that protrudes beyond the usually symmetric TDS. Later in the debris ejection process (right), the concentrated RFGFS moves around the TDS, pushing debris further from the TDS, characterized by an extended "tail" of low $\rho_{\rm HV}$.

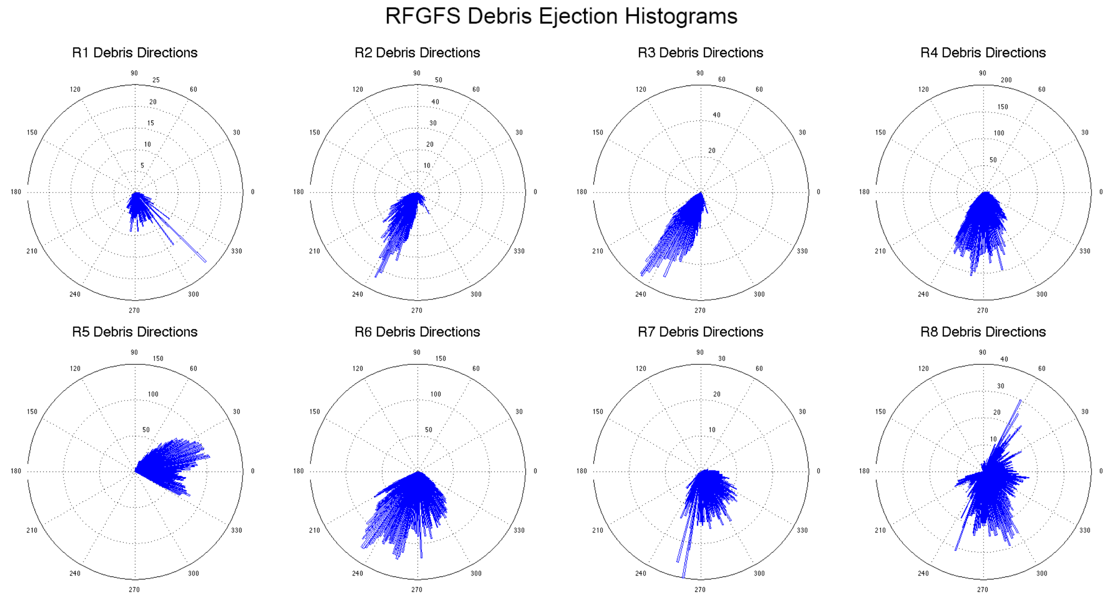

FIG. 3. Polar coordinate histograms of radar gates containing debris and their location relative to the center of the tornado (in a moving reference frame) for RFGFSs R1–R8. Magnitude is marked radially outward by number of gates, and direction (360 1° bins) indicates relative debris trajectory direction from the tornado. Each ejection plot is normalized, meaning the radial dimension changes from plot to plot.

locations are shown in polar coordinate histograms in Fig. 3.

b. Loop at Moore Medical Center

Although the loop at MMC is apparent in the PX-1000 data, there were a number of potentially related changes in storm structure observed in the minutes beforehand. In order to detail these changes, four sampling times have been selected for annotated presentation in Fig. 5, spanning from 2016:39–2026:16 UTC. These times are marked in Fig. 4 for reference along the track. Prior to 2016 UTC, a relatively mature mesocyclone-produced tornado had been ongoing for approximately 20 min (Fig. 1). Additionally, a Z_{DR} arc was evident from the forward flank to the base of the hook and around the TDS. Between 2014-2017 UTC, an area of high Z_{HH} ($\sim$60 dBZ), high Z_{DR} ($\sim$5 dB), and low ρ_{HV} ($\sim$.9) broke off from the rear/forward flank downdraft interface north of the tornado and moved southward toward the RFGF at a speed of 29 m s^{-1}.

The final stage of this southern surge can be seen in Fig. 5a. At this time, 2016:39 UTC, a strong v_r couplet, quasi-circular tornadic debris signature, and Z_{DR} arc were apparent as the mature tornado continued. At nearly the same time as the completing surge, the first area of EF5 damage occurred near Briarwood Elementary School, 2.75 km southwest of MMC. This period marked the beginning of a turn to the north-northeast, as indicated by the track in Fig. 4. In the forward flank, ρ_{HV} was relatively high, indicating primarily rain, but an area of lowered Z_{DR} was beginning to break into the Z_{DR} arc along the southern fringe of the forward flank downdraft (FFD).

Shortly afterwards, at 2020:37 UTC, the lowered Z_{DR} values in the forward flank showed a transition to the west, within the portion of the Z_{DR} arc closest to the updraft (Fig. 5b). This has been hypothesized by Kumjian et al. (2010) to indicate a disruption in the updraft and an occlusion process. Additionally, a large area of low ρ_{HV} was becoming evident on the southern flank of the FFD, possibly indicating debris fallout (Magsig and Snow 1998). Subsequently, the southern surge passed through the RFD, and resulted in a RFGFS (R4) and an associated debris ejection, visible in both Z_{HH} and ρ_{HV}

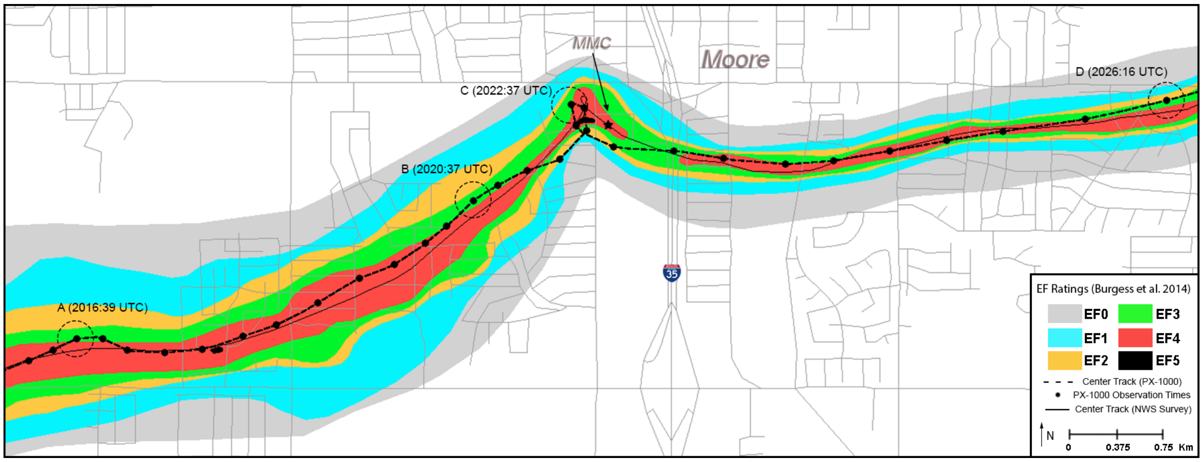

Fig. 4. EF-scale damage ratings (colored shading, from Burgess et al. (2014)), vortex center track from PX-1000 Δv_r data (dotted black line), and NWS damage survey center track (thin solid black line) for the loop area near the MMC (black star). Circled/labeled times A–D refer to the data presented in Fig. 5.

in Fig. 5b. In its wake, a distinct break in the hook echo to the northwest of the tornado became evident. The high Z_{DR} values in the southern surge had transitioned to lower values as debris was mixed in with the RFGFS, and the couplet had maintained its high Δv_r over the period. As can be seen in Fig. 3, R4 maintained a predominantly southern motion.

Two minutes later, at 2022:37 UTC, the lowered Z_{DR} values had mostly dissipated across the southern forward flank, but a break in the Z_{DR} arc had become apparent to the west of the hook (Fig. 5c). In the same area, a disrupted hook structure is present in Z_{HH}. The low ρ_{HV} intrusion in the FFD had shrunk in size but was still evident. A second and third RFGFS (R5 and R6) became evident in both Z_{HH} and ρ_{HV}, and the Δv_r had lowered from 125 m s^{-1} to 100 m s^{-1}, indicating a weakened couplet in v_r. RFGFS R5 displayed intensity and directional characteristics of an occluding RFD surge typically seen in occluding cyclic mesocyclogenesis (Fig. 3; Adlerman and Droegemeier (2005)), with large components of the debris ejection pointing to the northeast, possibly indicating an attempted occlusion of the tornadic circulation. R6, on the other hand, was oriented to the south, in a similar fashion to earlier RFGFSs. At this point, the tornado slowed to under 5 m s^{-1} and began to move toward the northwest, also a common characteristic of an occluding mesocyclone/tornado (Burgess et al. 1982; Adlerman et al. 1999; Dowell and Bluestein 2002).

At 2026:16 UTC (Fig. 5d), R6 had surged quickly southward and had primary debris ejection trajectories toward the south and south-southwest (Fig. 3). While the selected time of observation was past the time of the loop, it shows the debris associated with R5 being ejected to the northeast of the tornado while R6 surges to the south. At this time, the forward ground speed had increased to 9 m s^{-1}. Additionally, both the lowered Z_{DR} and ρ_{HV} values had recovered to the values seen during the mature stages before the loop. The Z_{DR} arc, specifically, had recovered to a fully mature state, and the hook echo was once again fully connected in Z_{HH}. A nearly symmetric TDS is evident in ρ_{HV}, and the remnant debris tail from R6 (and presumably previous RFGFSs) is clear in all moments.

5. Discussion

Multiple cyclic tornado studies have presented dissipating tornadoes that move along or near the occlusion point, resulting in motion toward the "rear" of the updraft (Dowell and Bluestein 2002; Houser 2013). In some cases, this has led to a nearly full loop of the tornado before eventual occlusion and dissipation occurs (Wurman et al. 2007; Bluestein et al. 2010; Tanamachi et al. 2012). Houser (2013) and Houser et al. (2014) show a hybrid case from 24 May 2011 in which it is hypothesized that the RFGFS remained contained without fully wrapping around the updraft, allowing the reorganizing meso-

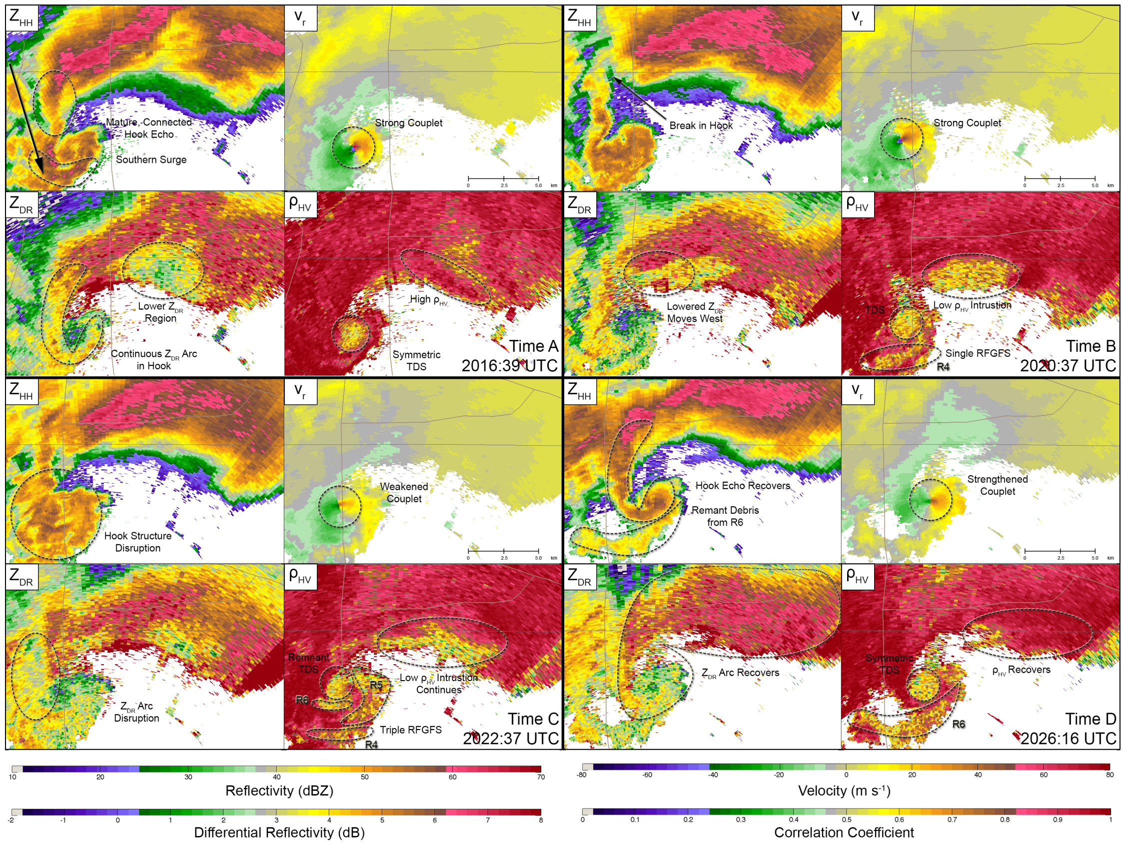

FIG. 5. Sample Z_{HH}, v_r, ρ_{HV}, and Z_{DR} data (clockwise from top left in each sub-frame) from different times/locations during the tornado loop period. Times are in reference to circles and times A-D in Fig. 4.

cyclone to keep access to warm inflow air. While this did allow the tornado to continue without immediate occlusion, dissipation did occur shortly thereafter.

As a potential explanation for what occurred in the Moore tornado, a hybrid conceptual diagram, adapted from the combination of PX-1000 data, Burgess et al. (1982), Dowell and Bluestein (2002), and the Houser (2013) case, is presented in Fig. 6. As the RFGFS associated with the occlusion (RFGFS 1) wraps RFD air around the updraft and tornado, the tornado begins to move to the north and eventually the northwest in an occlusion-type pattern. Near the apex of the northward turn, a secondary RFGFS, labeled RFGFS 2 in the diagram, pushes a new corridor of RFD air towards the south and southeast, in contrast to the predominant direction of RFGFS 1. This process may or may not result in a full loop, and could take place with more than two RFGFSs. RFGFSs 1 and 2 in the diagram are analogous to R5 and R6 in the Moore case, respectively.

The prevailing hypothesis is that initially, an imbalance of inflow and RFD winds causes the tornado to move north, similar to an occlusion process. However, with the strong southerly surge directly afterwards, the inflow and RFD wind balance changes and the vortex migrates southward, restoring the location of the tornado and preventing the occlusion of the tornado. This is similar to the tornadic mesocyclone cases described in Adlerman and Droegemeier (2005) and Houser (2013); however, the tornado and mesocyclone recover fully and continue on a path similar to that before the original northerly turn and in a relatively mature state. Additionally, depending on the strength, timing, and directivity of the secondary RFGFS, as well as any additional RFGFSs throughout the process, abrupt changes in forward ground speed may be observed, as with the

Moore case just past I-35.

We are referring to this process as a "failed occlusion" of the parent mesocyclone and tornado because of the apparent occlusion processes observed prior to the loop. As shown in Fig. 5, a number of events indicative of a weakening updraft, debris fallout, and an attempt at occlusion are evident. The southern surge of precipitation that preceded the northerly turn was followed by single-elevation observations of lowered Z_{HH} and Z_{DR}, possibly indicating fallout of large drops that were then transported rapidly south by the RFD. Such a development in the RFD would likely lead to an enhanced area of RFD winds, resulting in a RFGFS as indicated shortly after in R4. This hypothesis is also supported by the relatively high values of Z_{HH} and Z_{DR} in the southern surge (Fig. 5a).

6. Conclusions

The 20 May Moore tornado was observed by PX-1000 at high temporal resolution, allowing for analysis of various storm attributes that occurred on rapid time scales. The lack of volumetric dual-Doppler observations requires the use of polarimetric estimates to track RFD velocities and directions. Through this analysis, eight different RFGFSs marked by debris ejection patterns were identified during the lifetime of the tornado. Among the eight RFGFSs, three occurred in rapid succession, including the middle RFGFS that marked an apparent occlusion process with a debris ejection primarily angled to the northeast.

During the ongoing occlusion process, a second RFGFS aligned primarily to the south appeared to have provided enough balance between the supercellular inflow and outflow regimes to maintain the dominant mesocyclone and tornado structure, effectively "pushing" the tornado back onto an easterly path after the completion of a counter-clockwise looping trajectory. Afterwards, a significant increase in forward ground speed, coupled with a recovered updraft and tornadic vortex, allowed the tornado to continue for an additional 12 min, a time marked by

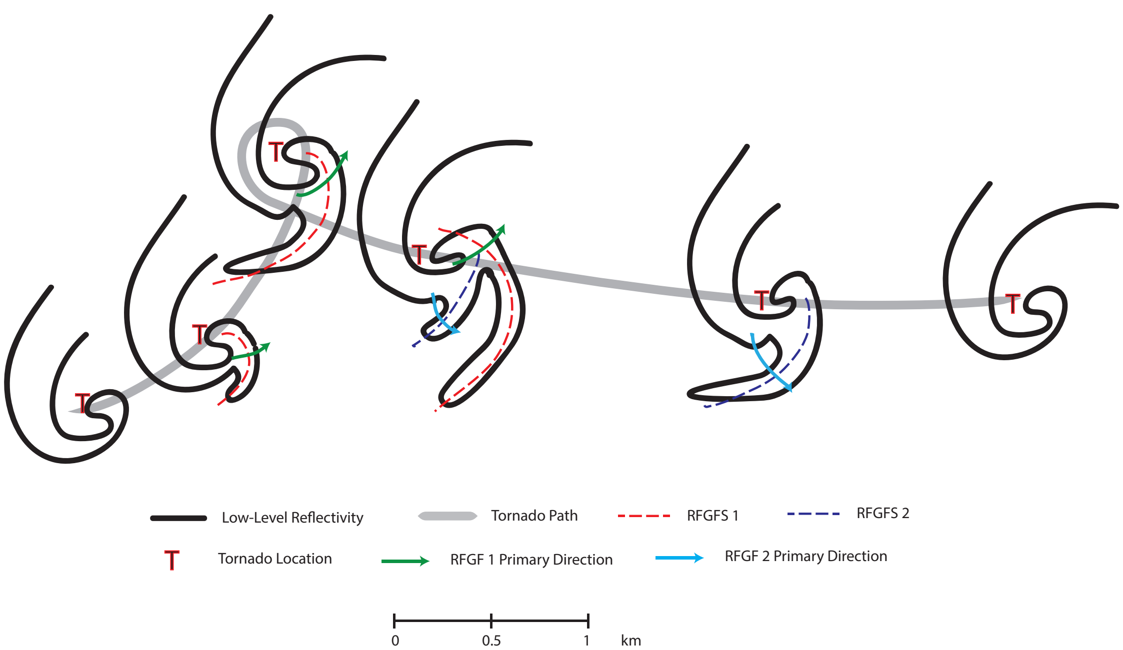

Fig. 6. Conceptual diagram of the failed occlusion process. The tornado and mesocyclone are first impacted by an occlusion-forcing RFGFS (RFGFS 1), which wraps around the tornado, causing a turn to the north. A second RFGFS (RFGFS 2) impinges upon the tornado near the apex of the loop with a predominantly southern direction relative to RFGFS 1, causing the tornado to move in a circular pattern and re-gain a steady state after a looped track. RFGFSs 1 and 2 are analogous to R5 and R6, respectively, in the Moore case.

consistent EF3 and common EF4 damage. This process, referred to as a failed occlusion, is thought to have been a result of a hybrid cyclic RFD process not yet seen in the literature. This hypothesis does not take into account thermodynamic data (which are not available for the storm in question), but serves as one possible explanation for the observations.

Acknowledgments.

This work was supported by the National Science Foundation under grant AGS1303685. The authors would like to thank Don Burgess and Jeff Snyder for their detailed review of the dataset and analysis techniques. Greg Stumpf, Rick Smith, and Gabe Garfield provided valuable discussions regarding the NWS damage survey of the 20 May Moore tornado.

REFERENCES

Adlerman, E. J. and K. K. Droegemeier, 2005: The dependence of numerically simulated cyclic mesocyclogenesis upon environmental vertical wind shear. *Mon. Wea. Rev.*, **133 (12)**, 3595–3623.

Adlerman, E. J., K. K. Droegemeier, and R. Davies-Jones, 1999: A numerical simulation of cyclic mesocyclogenesis. *J. Atmos. Sci.*, **56 (13)**, 2045–2069.

Atkins, N. T., K. M. Butler, K. R. Flynn, and R. M. Wakimoto, 2014: An integrated damage, visual, and radar analysis of the 2013 Moore Oklahoma EF5 tornado. *Bull. Amer. Meteor. Soc.*, in press.

Bluestein, H. B., M. M. French, I. PopStefanija, R. T. Bluth, and J. B. Knorr, 2010: A mobile, phased-array Doppler radar for the study of severe convective storms. *Bull. Amer. Meteor. Soc.*, **91 (5)**, 579–600.

Bodine, D. J., M. R. Kumjian, R. D. Palmer, P. L. Heinselman, and A. V. Ryzhkov, 2013: Tornado damage estimation using polarimetric radar. *Wea. Forecasting*, **28 (1)**, 139–158.

Bringi, V. N., V. Chandrasekar, N. Balakrishnan, and D. S. Zrnić, 1990: An examination of propagation effects in rainfall on radar measurements at microwave frequencies. *J. Atmos. Oceanic Technol.*, **7**, 829–840.

Burgess, D., et al., 2014: 20 May 2013 Moore, Oklahoma tornado: Damage survey and analysis. *Wea. Forecasting*, **29 (5)**, 1229–1237.

Burgess, D. W., V. T. Wood, and R. A. Brown, 1982: Mesocyclone evolution statistics. *Preprints, 12th Conf. on Severe Local Storms*, San Antonio, TX, Amer. Meteor. Soc., 422–424.

Cheong, B. L., R. Kelley, R. D. Palmer, Y. Zhang, M. Yeary, and T.-Y. Yu, 2013: PX-1000: A solid-state polarimetric X-band weather radar and time-frequency multiplexed waveform for blind range mitigation. *IEEE Trans. Instrum. Meas.*, **62 (11)**, 3064–3072.

Dowell, D. C. and H. B. Bluestein, 2002: The 8 June 1995 Mclean, Texas, storm. Part I: Observations of cyclic tornadogenesis. *Mon. Wea. Rev.*, **130 (11)**, 2626–2648.

Finley, C. A. and B. D. Lee, 2004: High resolution mobile mesonet observations of RFD surges in the June 9 Basset, Nebraska supercell during Project ANSWERS 2003. *Preprints, 22nd Conf. on Severe Local Storms*, Hyannis, MA, Amer. Meteor. Soc., P11.3.

Houser, J. B., 2013: Observations of supercell tornado evolution using a mobile, rapid-scan, X-band radar. Ph.D. thesis, University of Oklahoma.

Houser, J. B., H. B. Bluestein, and J. C. Snyder, 2014: Rapid-scan, polarimetric, Doppler-radar observations of tornadogenesis and tornado dissipation in a tornadic supercell: The "El Reno, Oklahoma" storm of 24 May 2011. *Mon. Wea. Rev.*, accepted pending revisions.

Jameson, A. R., 1992: The effect of temperature on attenuation-correction schemes in rain using polarization propagation differential phase shift. *J. Appl. Meteor.*, **31 (9)**, 1106–1118.

Kumjian, M. R., A. V. Ryzhkov, V. M. Melnikov, and T. J. Schuur, 2010: Rapid-scan super-resolution observations of a cyclic supercell with a dual-polarization WSR-88D. *Mon. Wea. Rev.*, **138 (10)**, 3762–3786.

Kurdzo, J. M., B. L. Cheong, R. D. Palmer, G. Zhang, and J. Meier, 2014: A pulse compression waveform for improved-sensitivity weather radar observations. *J. Atmos. Oceanic Technol.*, in press.

Magsig, M. A. and J. T. Snow, 1998: Long-distance debris transport by tornadic thunderstorms. Part I: The 7 May 1995 supercell thunderstorm. *Mon. Wea. Rev.*, **126 (6)**, 1430–1449.

Park, S. G., V. N. Bringi, V. Chandrasekar, M. Maki, and K. Iwanami, 2005: Correction of radar reflectivity and differential reflectivity for rain attenuation at X band. Part I: Theoretical and empirical basis. *J. Atmos. Oceanic Technol.*, **22**, 1621–1632.

Ryzhkov, A., D. Burgess, D. Zrnić, T. Smith, and S. Giangrande, 2002: Polarimetric analysis of a 3 May 1999 tornado. *Preprints, 21st Conf. on Severe Local Storms*, San Antonio, TX, Amer. Meteor. Soc., 14.2.

Ryzhkov, A. V., T. J. Schurr, D. W. Burgess, and D. Zrnić, 2005: Polarimetric tornado detection. *J. Appl. Meteor. Climatol.*, **44**, 557–570.

Skinner, P. S., C. C. Weiss, M. M. French, H. B. Bluestein, P. M. Markowski, and Y. P. Richardson, 2014: VORTEX2 observations of a low-level mesocyclone with multiple internal rear-flank downdraft momentum surges in the 18 May 2010, Dumas, Texas supercell. *Mon. Wea. Rev.*, **142 (8)**, 2935–2960.

Snyder, J. C., H. B. Bluestein, G. Zhang, and S. J. Frasier, 2010: Attenuation correction and hydrometeor classification of high-resolution, X-band, dual-polarized mobile radar measurements in severe convective storms. *J. Atmos. Oceanic Technol.*, **27 (12)**, 1979–2001.

Tanamachi, R. L., H. B. Bluestein, J. B. Houser, S. J. Frasier, and K. M. Hardwick, 2012: Mobile, X-band, polarimetric Doppler radar observations of the 4 May 2007 Greensburg, Kansas, tornadic supercell. *Mon. Wea. Rev.*, **140 (7)**, 2103–2125.

Wurman, J., Y. Richardson, C. Alexander, S. Weygandt, and P. F. Zhang, 2007: Dual-Doppler and single-Doppler analysis of a tornadic storm undergoing mergers and repeated tornadogenesis. *Mon. Wea. Rev.*, **135 (3)**, 736–758.